

Femtosecond rotational dynamics of D₂ molecules in superfluid helium nanodroplets

Junjie Qiang,^{1,*} Lianrong Zhou,^{1,*} Peifen Lu,^{1,†} Kang Lin,¹ Yongzhe Ma,¹ Shengzhe Pan,¹ Chenxu Lu,¹ Wenyu Jiang,¹ Fenghao Sun,¹ Wenbin Zhang,¹ Hui Li,¹ Xiaochun Gong,¹ Ilya Sh. Averbukh,² Yehiam Prior,^{1,2} Constant A. Schouder,³ Henrik Stapelfeldt,^{3,‡} Igor N. Cherepanov,⁴ Mikhail Lemeshko,⁴ Wolfgang Jäger,⁵ Jian Wu^{1,6,7,§}

¹*State Key Laboratory of Precision Spectroscopy, East China Normal University, Shanghai 200241, China*

²*AMOS and Department of Chemical Physics, Weizmann Institute of Science, Rehovot 76100, Israel*

³*Department of Chemistry, Aarhus University, Langelandsgade 140, 8000 Aarhus C, Denmark*

⁴*Institute of Science and Technology Austria, Am Campus 1, 3400 Klosterneuburg, Austria*

⁵*Department of Chemistry, University of Alberta, Edmonton, Alberta T6G 2G2, Canada*

⁶*Collaborative Innovation Center of Extreme Optics, Shanxi University, Shanxi 030006, China*

⁷*CAS Center for Excellence in Ultra-intense Laser Science, Shanghai 201800, China*

Abstract

Rotational dynamics of D₂ molecules inside helium nanodroplets is induced by a moderately intense femtosecond (fs) pump pulse and measured as a function of time by recording the yield of HeD⁺ ions, created through strong-field dissociative ionization with a delayed fs probe pulse. The yield oscillates with a period of 185 fs, reflecting field-free rotational wave packet dynamics, and the oscillation persists for more than 500 periods. Within the experimental uncertainty, the rotational constant B_{He} of the in-droplet D₂ molecule, determined by Fourier analysis, is the same as B_{gas} for an isolated D₂ molecule. Our observations show that the D₂ molecules inside helium nanodroplets essentially rotate as free D₂ molecules.

* These two authors contributed equally.

† pflu@lps.ecnu.edu.cn

‡ henriks@chem.au.dk

§ jwu@phy.ecnu.edu.cn

Laser-induced alignment of molecules in the gas phase has been intensively studied in the last decades and used in various applications [1-6]. In particular, moderately intense femtosecond laser pulses can create rotational wave packets, i.e., coherent superpositions of field-free rotational eigenstates, leading to alignment and anti-alignment revivals in narrow, periodically-occurring time windows. For isolated linear and symmetric top molecules, the characteristic revival structure of the time-dependent degree of alignment, explored in a large number of works, persists and does not change provided coupling of the rotational angular momentum to, e.g., the nuclear spin is negligible [7, 8]. On the other hand, if the molecules are in dense gas, collisions with other molecules or atoms will lead to a gradual dephasing of the wave packet and possibly rotational redistribution, which manifests as gradual disappearance of the revival structures [9-11].

Recently, alignment in the short-pulse or nonadiabatic regime (limit) was extended to molecules embedded in liquid helium nanodroplets [12-16]. Studies on OCS, CS₂ and I₂ molecules showed that when their rotational energy is kept well below the roton energy of the droplet [17, 18], where coupling between rotation and the phonons is weak, revivals are present in the time-dependent degree of alignment traces, reflected as discrete peaks in the corresponding frequency spectra. These observations were interpreted as a consequence of the superfluidity of He droplets. Although the observed rotational dynamics differed strongly from the rotational dynamics of gas-phase molecules, a free-rotor model accounted for the experimental results [15]. It revealed that the difference is due to the smaller effective rotational constant B_{He} and the much larger centrifugal distortion constant D_{He} of the in-droplet molecules [17, 18] compared to those of the gas-phase molecules, B_{gas} and D_{gas} , as well as to a distribution rather than a single value of B_{He} and D_{He} .

For OCS, CS₂ and I₂, the $B_{\text{gas}}/B_{\text{He}}$ ratio lies between 2 and 5, an effect caused by a nonsuperfluid density of He corotating with the molecules [19]. For smaller and lighter molecules, corresponding to larger values of B_{gas} , $B_{\text{gas}}/B_{\text{He}}$ tends towards 1, notably when $B_{\text{gas}} > 1 \text{ cm}^{-1}$. This trend, qualitatively explained as the surrounding He

atoms not being able to follow the fast-rotating molecules, indicates that the rotation of small molecules inside He droplets should closely resemble that in the gas phase. However, the collected information from a large number of Infrared (IR) spectroscopy studies have established a correlation between D_{He} and B_{He} , expressed as $D_{\text{He}} = 0.038B_{\text{He}}^{1.88}$ (using cm^{-1} units) [18]. If this correlation remains valid for $B_{\text{He}} > 1 \text{ cm}^{-1}$, then D_{He} becomes comparable to B_{He} , a situation that will lead to rotational dynamics very different from that of gas-phase molecules. On the other hand, the quasiparticle angulon model recently predicted that in the limit of light rotors, D_{He} scales as B_{He}^{-1} , thereby deviating from the nearly quadratic dependence [16]. Using the reported analytic formula, we estimate the upper bound of $D_{\text{He}} = 0.001 \text{ cm}^{-1}$ for D_2 (see Supplemental Material [20], Sec. V). So an obvious question arises: How do small and light molecules ($B_{\text{gas}} \gg 1 \text{ cm}^{-1}$) rotate inside superfluid He droplets? The purpose of this Letter is to answer this question. It is done by using a non-resonant fs pulse to create rotational wave packets in D_2 molecules embedded in helium nanodroplets and measuring the rotational dynamics through timed strong-field ionization. The observed rotational dynamics is essentially the same as that of isolated gas-phase D_2 molecules.

A schematic of the experimental setup is given in Fig. 1(a). A continuous helium nanodroplet beam was produced by expanding pre-cooled (16.2 K), high purity (99.9999%), ^4He gas at 20 bar stagnation pressure through a 5- μm -diameter nozzle. The average size of the droplets is estimated to be 2000 atoms [17]. The helium nanodroplets were doped by passing through a 4-cm-long pick-up cell containing D_2 molecules. Two orthogonally-polarized pulsed laser beams were focused by a concave silver mirror ($f=7.5 \text{ cm}$) onto the D_2 -doped He droplets in the reaction microscope of a Cold Target Recoil Ion Momentum Spectroscopy (COLTRIMS) setup [21, 22]. The parameters of the pulses in the pump beam, used to induce alignment, were 790 nm, $\sim 40 \text{ fs}$, y -polarized, and the parameters of the beam used to probe the alignment, were 395 nm, $\sim 30 \text{ fs}$, z -polarized. The peak intensities of the pump and the probe pulses in the interaction region were estimated to be $I_{\text{pump}} = 8.0 \times 10^{13} \text{ W/cm}^2$ and $I_{\text{probe}} =$

$2.0 \times 10^{14} \text{ W/cm}^2$.

In previous studies of laser-induced alignment of molecules in He droplets, the degree of alignment was measured by Coulomb exploding the molecules with an intense laser pulse and recording the emission directions of the fragment ions [12, 23]. Fragment ions like I^+ , Br^+ , or S^+ from, e.g., I_2 , $\text{C}_6\text{H}_5\text{Br}$ and CS_2 molecules, respectively, lose some of their initial directionality following the Coulomb explosion event due to scattering on He atoms as the ions move out of the droplet, but their final angular distribution can still be used to determine the degree of alignment [23, 24]. For the much lighter fragment ion D^+ , the influence of the He scattering on the ion trajectories is more severe, and our experiment shows that the Coulomb explosion probe method is not well-suited (see Supplemental Material [20], Sec. I). Instead, the rotational dynamics is probed by ionizing the D_2 molecules with the probe pulse and measuring the dissociative-ionization yield because it depends on the orientation of the molecular axis relative to the polarization of the probe pulse.

The alignment-dependent dissociative ionization process details are illustrated in Fig. 1(b). The probe pulse ionizes and dissociates the D_2 molecule via two channels: $\text{D}_2 \rightarrow \text{D}_2^+ + e \rightarrow \text{D}^+ + \text{D} + e$, denoted as $\text{D}_2(1,0)$ and $\text{D}_2 \rightarrow \text{D}_2^+ + e \rightarrow \text{D}^+ + \text{D}^+ + 2e$, denoted as $\text{D}_2(1,1)$. Both channels are sequential, and the first step is multiphoton ionization of D_2 . The ionization step depends only mildly on the molecular alignment [25, 26]. For the $\text{D}_2(1,0)$ channel, the second step is a parallel transition between the $1\sigma_g$ and $2p\sigma_u$ states of D_2^+ [27], while for the $\text{D}_2(1,1)$ channel, the second step is dominated by charge-resonance-enhanced ionization of D_2^+ [28]. Both of these two processes occur most effectively when the molecular axis aligns along the polarization direction of the laser pulse, i.e., they are alignment-dependent. As a result, the rotational dynamics can be visualized by measuring the time-dependent yield of the dissociative ionization channels [29, 30], i.e., the D^+ ion yield, with the highest (lowest) yield expected when the molecules align parallel (perpendicular) to the probe polarization.

The laser pulses interacted not only with D_2 molecules inside He droplets but also with free D_2 molecules that diffused from the pickup cell to the target region. To

eliminate the background contribution from these isolated D_2 molecules and obtain a signal that exclusively originates from D_2 molecules embedded in the droplets, we recorded HeD^+ ions rather than D^+ ions. This strategy is similar to that employed in past studies on, e.g., I_2 molecules where HeI^+ ions were recorded [14, 23]. The HeD^+ ions stem from, we believe, D^+ fragment ions binding to a He atom as they travel out of the droplet.

Figure 1(c) depicts the measured position y-TOF spectrum of the ions produced by the probe pulse. The spectrum consists of two series of singly charged ionic fragments with mass-to-charge ratio $m/q = 4n$ and $m/q = 4n+2$ ($n = 1, 2, 3, 4, \dots$), which are respectively assigned to He_n^+ and He_nD^+ ions [31]. The $m/q=4n$ may also have a contribution from $He_{n-1}D_2^+$ ions. The signals with $1000 \text{ ns} < \text{TOF} < 2000 \text{ ns}$ are mainly from D^+ ions produced when D_2 molecules are dissociatively ionized. In what follows, we focus on the peak with $m/q=6$ (marked by the dashed ellipse), which is assigned to HeD^+ ions and could only have originated from a D_2 molecule embedded in a helium droplet, as discussed above.

Figure 2(a) depicts the yield of the HeD^+ ions as a function of the kinetic energy (E_{kin}) and the time delay between the pump and the probe pulses. The time interval recorded was from -200 fs to 1000 fs with a step size of 6.7 fs. The E_{kin} axis is on a logarithmic scale, and the yield is normalized for each kinetic energy. Pronounced oscillation structures are visible with an apparent π -phase shift between ions with $0.1 \text{ eV} < E_{\text{kin}} < 1.0 \text{ eV}$ and ions with $E_{\text{kin}} < 0.04 \text{ eV}$. The yields integrated over the two E_{kin} ranges from 100 fs to 1000 fs are plotted in Fig. 2(b). The π -phase shift is evident, and it is seen that the two traces have the same oscillation period of $\sim 185 \text{ fs}$. Here, we focus on the high- E_{kin} fragments, i.e., HeD^+ , and discuss the low- E_{kin} in Supplemental Material [20], Sec. II.

To explore the further evolution of the yield of the high- E_{kin} ions, measurements were conducted in the interval 1–7 ps with a step size of 10 fs. Figure 3(a) shows that the oscillations in the yield continue essentially without any change, a behavior qualitatively different from the alignment dynamics previously observed for I_2 , CS_2

and OCS embedded in He droplets [15]. The regular sine-like structure of the yield indicates that the D₂ rotational dynamics is the result of a wave packet dominated by two rotational quantum states [32]. To investigate if that is the case, the time-dependent HeD⁺ yield from 1 ps to 7 ps was Fourier transformed. The power spectrum, represented by the red curve in Fig. 3(c), contains three peaks, of which the one centered at 5.35 THz is the dominant one.

Like past studies on both isolated and in-droplet molecules, one may expect that the central value of each spectral peak is given by the frequency of a ($J-J+2$) coherence in the rotational wave packets created by the alignment pulse, where J is the rotational angular momentum. Consequently, we assign the three observed peaks at 5.35, 8.92, and 12.40 THz as the (0–2), (1–3), and (2–4) coherences, respectively. The observation that the 5.35 THz peak is by far the strongest shows that this frequency dominates the rotational dynamics. This is consistent with the observed period of ~185 fs in the time-dependent yield of HeD⁺.

In Fig. 3(d), the central frequencies of the spectral peaks are plotted as a function of J . In analogy with previous studies, we fit the data points to $B(4J + 6) - D(8J^3 + 36J^2 + 60J + 36)$, which is the expression for the frequencies of the ($J - J+2$) coherences for a non-rigid linear molecule, characterized by the rotational constant B and the centrifugal distortion constant D [15]. The best fit, shown by the red curve in Fig. 3(d) is obtained for $B_{\text{He}} = 29.9 \pm 1.3 \text{ cm}^{-1}$ and $D_{\text{He}} = 0.013 \pm 0.060 \text{ cm}^{-1}$, with units converted from THz to cm^{-1} (see the discussion on uncertainty in Supplemental Material [20], Sec. III). There is a large relative uncertainty in both B_{He} and D_{He} because the fit is based only on three points. In particular, for D_{He} , the uncertainty is larger than the central value but the result still shows that $D_{\text{He}} \ll B_{\text{He}}$ and allows us to conclude that the $D_{\text{He}} = 0.038B_{\text{He}}^{1.88}$ correlation [18] does not apply to D₂ molecules. Moreover, the above mentioned estimate $D_{\text{He}} = 0.001 \text{ cm}^{-1}$ lies within the uncertainty range. Our results are the first measured values of B_{He} and D_{He} for D₂ molecules embedded in He droplets.

As a reference, the time-dependent yield for isolated D₂ molecules in the

background, measured using D^+ as the observable (blue curve in Fig. 3(b)), exhibits an oscillatory structure similar to that of the HeD^+ in Fig. 3(a). The corresponding power spectrum, shown by the blue curve in Fig. 3(c), contains four peaks which we assign as the (0–2), (1–3), (2–4) and (3–5) coherences, respectively. The central positions of the spectral peaks, of which the first three essentially coincide with those for the D_2 molecules in He droplets, are plotted as a function of J in Fig. 3(e). Again, the experimental data points are fitted to the non-rigid rotor expression, and we find that the best fit, represented by the blue curve, is obtained for $B_{\text{gas}} = 29.98 \pm 0.13 \text{ cm}^{-1}$, $D_{\text{gas}} = 0.013 \pm 0.004 \text{ cm}^{-1}$. Within the uncertainty of the experiment, these results are consistent with the values, 29.91 cm^{-1} and 0.01123 cm^{-1} obtained from either experimental spectroscopic measurements or theoretical calculations of the rovibrational spectra of isolated gas-phase D_2 molecules [33-35].

Figure 3(c) shows that the relative intensities of the spectral peaks are not the same for the isolated and the in-droplet D_2 molecules. As we now explain, this is ascribed to a difference in the initial population, $P(J)$, of the rotational states. For the isolated D_2 molecules, $P(J)$ is determined by a Boltzmann distribution with a rotational temperature, T_{rot} , equal to 295 K and taking into account the 2:1 nuclear spin statistical factor for the even (ortho- D_2) and odd (para- D_2) states: $P(0) = 19\%$, $P(1) = 21\%$, $P(2) = 39\%$, $P(3) = 11\%$, $P(4) = 9\%$, $P(5) = 1\%$. With this population distribution, the parameters of the experimental alignment pulse, and the B_{gas} and D_{gas} values from the fit of the experimental data, we calculated $\langle \cos^2 \theta \rangle(t)$, the standard metric for the degree of alignment, by solving the time-dependent rotational Schrödinger equation; here, θ is the angle between the alignment pulse polarization and the D_2 internuclear axis. Subsequently, Fourier transforming $\langle \cos^2 \theta \rangle(t)$ gives a spectrum that is very close to the blue curve in Fig. 3(c) (see Supplemental Material [20], Sec. IV). If $P(J)$ for the in-droplet D_2 molecules is determined by a Boltzmann distribution with $T_{\text{rot}} = 0.37 \text{ K}$ as observed for molecules like SF_6 [36], OCS [37], CS_2 and I_2 [23], then only the $J = 0$ state should be populated. Only spectral peaks from coherences between states with even J values would be seen. The observation of the

(1–3) peak in Fig. 3(c) shows that some of the D_2 molecules inside the droplets are initially populated in states with odd J . Consequently, the time it takes a He droplet to fly from the pickup cell, where the D_2 molecules are embedded, to the interaction region with the laser beam, about 2.2 ms in our experiment, is not sufficient to completely thermalize the rotational state distribution initially at 295 K to one at 0.37 K. We believe this is due to the well-known long time scales for flipping the nuclear spin of the deuterons [38–40].

The information from the time-dependent HeD^+ yield and the corresponding power spectrum allows us to conclude that the laser-induced rotational dynamics of the D_2 molecules inside He droplets is determined mainly by the (0–2) coherence with frequency 5.35 THz. The unchanged amplitude of HeD^+ in the 1–7 ps interval shows that inhomogeneous and homogeneous broadenings are negligible on this time scale. To explore dynamics on longer time scales, data were recorded in the intervals 19.42–20.02 ps and 100.1–100.7 ps, see Figs. 2(c)–(d). Due to the significant acquisition times required, the measurements were restricted to these two selected time windows. Again, the D^+ signal from isolated molecules was recorded as a reference. The signals measured in both time intervals demonstrate that the 185-fs oscillations are still present, even after 100 ps, although with a somewhat reduced amplitude compared to the first 7 ps. These observations show that the dominant (0–2) coherence of the rotational wave packet is preserved for more than 500 oscillations and that the $J = 2$ state has a lifetime of at least 100 ps. This is in accordance with a recent theoretical study investigating the influence of the rotational constants, the initial excited rotational state, and the droplet size on the rotational relaxation quantum dynamics of fast rotors inside helium nanodroplets [41]. The calculations predicted that the rotational relaxation of D_2 ($J = 2$, $M_J = 0$) in superfluid helium nanodroplets could be particularly slow (> 5 ns) due to the weak molecule-helium interaction. Here, we suggest that the low density of states of superfluid helium [42, 43] at the energies of the excited rotational states of D_2 may be responsible for the weak coupling of the molecular rotation with the superfluid helium excitations.

In summary, we experimentally investigated laser-induced field-free molecular alignment dynamics of D₂ molecules inside He droplets by measuring the time-dependent yield of HeD⁺ ions created by ionization with an intense probe laser pulse. The dominant (0–2) rotational coherence has energy (179 cm⁻¹) much above the roton energy of the droplets and persists for longer than 100 ps. From the power spectra of the alignment traces, B_{He} is determined and found to be the same as B_{gas}. In total, our measurements show that for at least 100 ps, equivalent to > 500 rotational periods, D₂ molecules in He droplets rotate as if they were isolated gas-phase particles. This behavior is strikingly different from the in-droplet rotation of all other molecules studied [44]. It would be interesting to investigate the rotational dynamics for significantly longer times to find out when coupling between the D₂ rotation and the droplet becomes important. This is in principle possible with our technique. So is studies on other light molecules like HF and C₂H₂, which would explore the rotational dynamics of rotors in the gap between the superlight D₂ and the heavier species like OCS.

This work is supported by the National Key R&D Program of China (Grant No. 2018YFA0306303); the National Natural Science Fund (Grants Nos. 11834004, 11621404 and 12174109); the project supported by the Shanghai Committee of Science and Technology (Grant No. 19JC1412200). J. Q. acknowledges support by ECNU Cultivation Project of Future Scientist & Outstanding Scholar (Grant No. WLKXJ202003). H. S. acknowledges support from the Villum Foundation through a Villum Investigator Grant No. 25886. M. L. acknowledges support by the European Research Council (ERC) Starting Grant No. 801770 (ANGULON). I. C. acknowledges support by the European Union's Horizon 2020 research and innovation programme under the Marie Skłodowska-Curie Grant Agreement No. 665385.

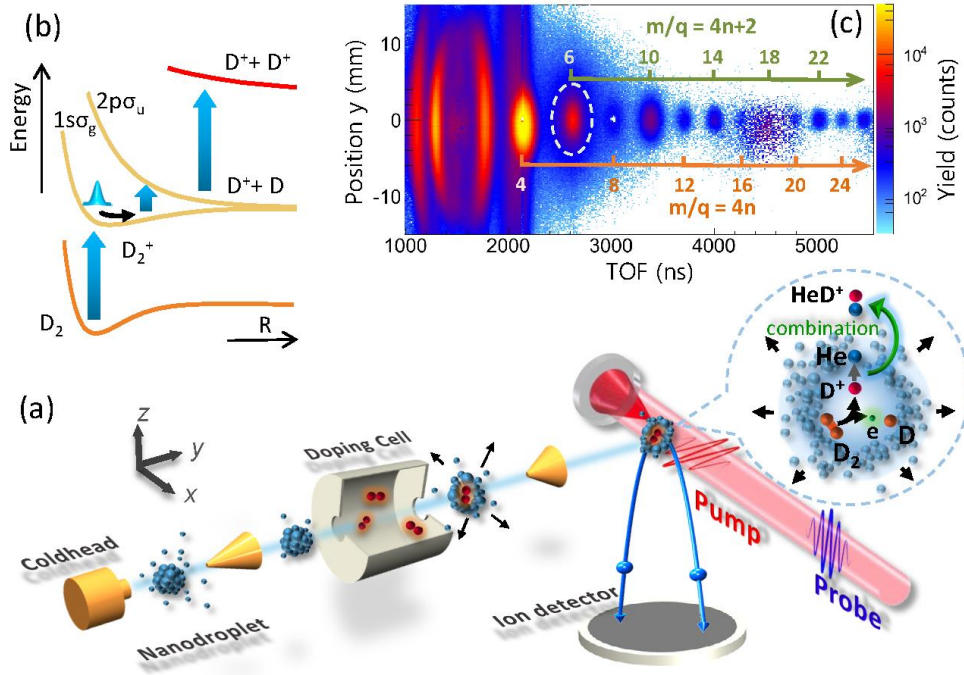


FIG. 1. (a) Schematic diagram of the experimental setup. The pump pulse initiates the rotational dynamics of D₂ molecules inside the He nanodroplets, and then the dynamics is measured through dissociative ionization, induced by the probe pulse, and recording of the HeD⁺ ions. (b) Sketch of relevant potential energy curves of D₂, D₂⁺ and D₂²⁺ (1/R Coulomb potential). The blue vertical arrows illustrate the two involved dissociative ionization channels, i.e., D₂(1,0) and D₂(1,1), see text. (c) Measured position y-TOF spectrum of the ions produced when the probe pulse interacts with the helium nanodroplets doped with D₂ molecules. The signal originating from the residual gas in the interaction chamber (e.g., H₂, H₂O and N₂), recorded when the jet of the pick-up cell was closed, was subtracted from the spectrum for clarity.

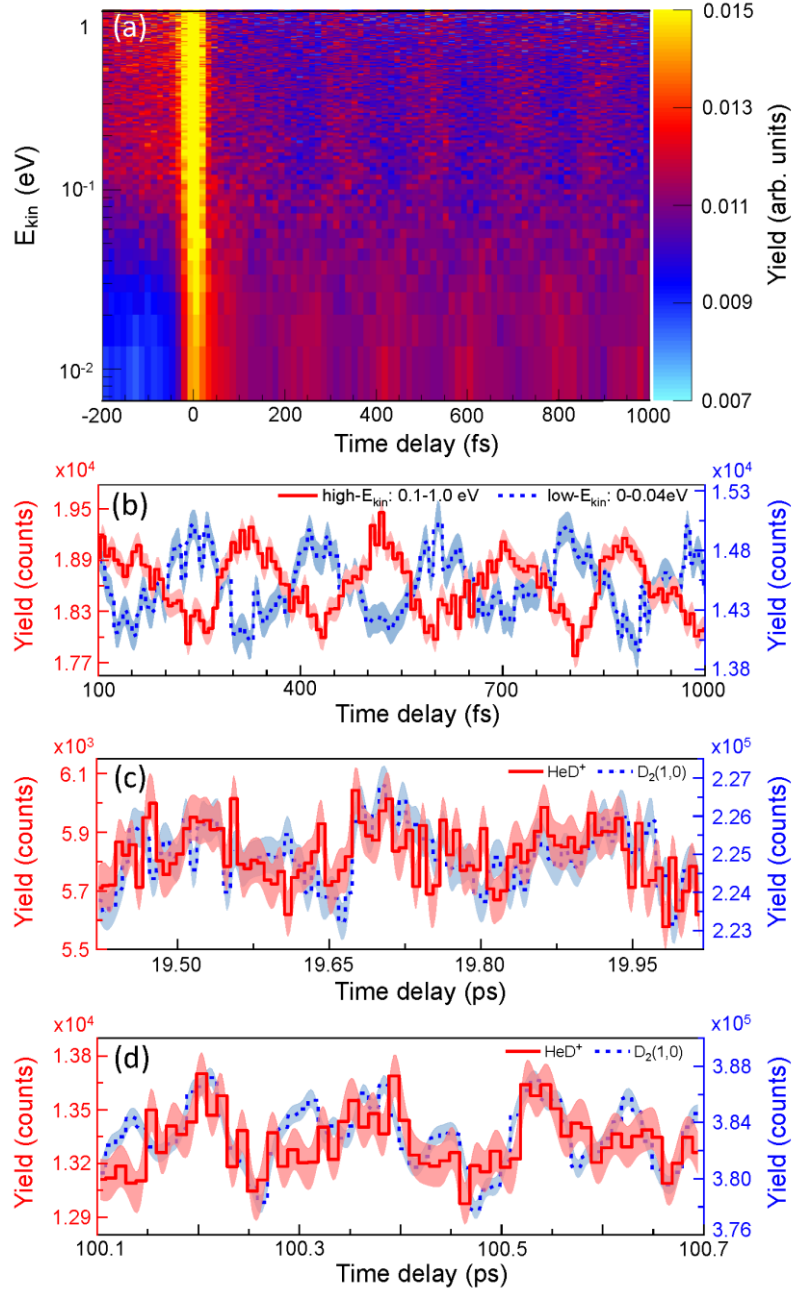


FIG. 2. (a) Yield of the ionic fragments with $m/q=6$ as a function of the kinetic energy and the time delay. (b) Time-dependent yield obtained by integrating the yield over the low- E_{kin} and the high- E_{kin} ranges. (c)-(d) Time-dependent yields of HeD^+ (from D_2 in He droplets) and D^+ (from the $\text{D}_2(1,0)$ channel of the isolated gas-phase D_2 molecules) in two selected time intervals. The shaded area represents the error bars. The time step sizes for the intervals of 19.42-20.02 ps and 100.1-100.7 ps are 6.7 fs and 10 fs, respectively.

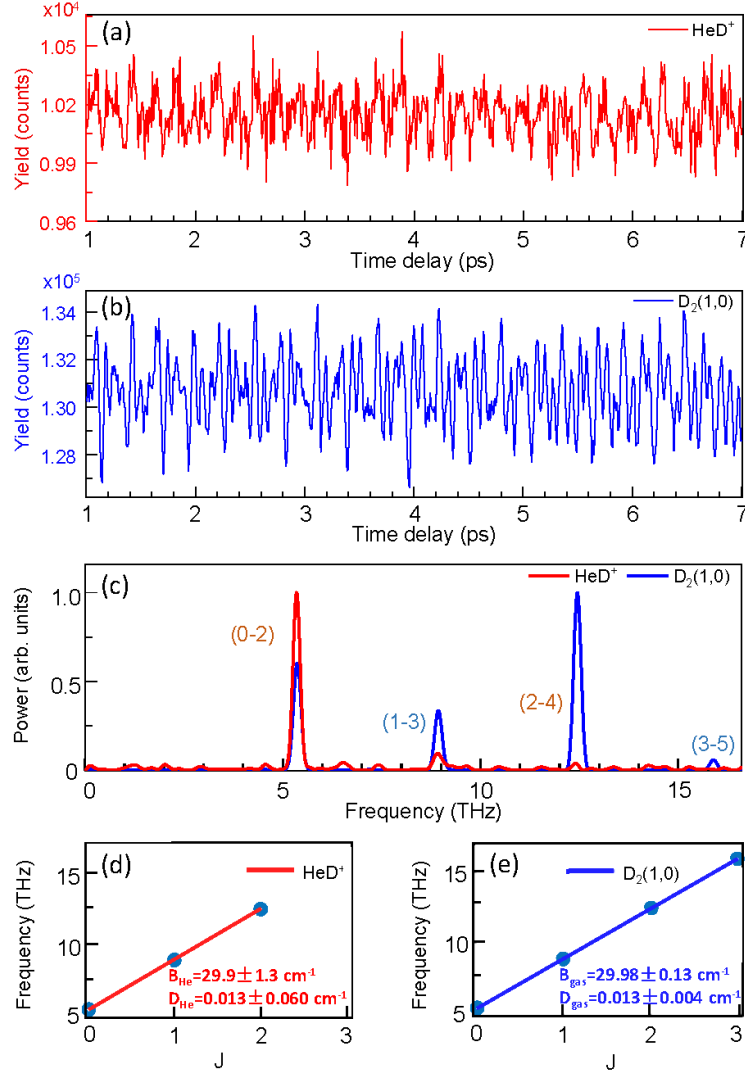


FIG. 3. (a)-(b) Time-dependent yields of HeD⁺ (from D₂ in He droplets) and D⁺ (from the D₂(1,0) channel of the gas-phase D₂ molecules) in the 1-7 ps time interval. (c) Power spectra of the yield traces in (a) and (b). (d)-(e) Central frequencies of $(J - J+2)$ peaks in the power spectra versus J . The full lines represent the best fits using the least square method; see text. The B and D constants from the fits are given with 95% confidence bounds for the in-droplet D₂ molecules and the isolated gas-phase D₂ molecules.

References

- [1] H. Stapelfeldt and T. Seideman, Colloquium: Aligning molecules with strong laser pulses, *Rev. Mod. Phys.* **75**, 543 (2003).
- [2] C. P. Koch, M. Leshko, and D. Sugny, Quantum control of molecular rotation, *Rev. Mod. Phys.* **91**, 035005 (2019).
- [3] S. Fleischer, Y. Khodorkovsky, E. Gershnabel, Y. Prior, and I. S. Averbukh, Molecular alignment induced by ultrashort laser pulses and its impact on molecular motion, *Isr. J. Chem.* **52**, 414 (2012).
- [4] J. J. Larsen, I. Wendt-Larsen, and H. Stapelfeldt, Controlling the branching ratio of photodissociation using aligned molecules, *Phys. Rev. Lett.* **83**, 1123 (1999).
- [5] J. Maurer, D. Dimitrovski, L. Christensen, L. B. Madsen, and H. Stapelfeldt, Molecular-frame 3D photoelectron momentum distributions by tomographic reconstruction, *Phys. Rev. Lett.* **109**, 123001 (2012).
- [6] Jochen Küpper *et al.*, X-ray diffraction from isolated and strongly aligned gas-phase molecules with a free-electron laser, *Phys. Rev. Lett.* **112**, 083002 (2014).
- [7] E. F. Thomas, A. A. Søndergaard, B. Shepperson, N. E. Henriksen, and H. Stapelfeldt, Hyperfine-structure-induced depolarization of impulsively aligned I_2 molecules, *Phys. Rev. Lett.* **120**, 163202 (2018).
- [8] L. V. Thesing, A. Yachmenev, R. González-Férez, and J. Küpper, The effect of nuclear-quadrupole coupling in the laser-induced alignment of molecules, *J. Phys. Chem. A* **124**, 2225 (2020).
- [9] J. Ma, H. Zhang, B. Lavorel, F. Billard, E. Hertz, J. Wu, C. Boulet, J. -M. Hartmann, and O. Faucher, Observing collisions beyond the secular approximation limit, *Nat. Commun.* **10**, 5780 (2019).
- [10] T. Vieillard, F. Chaussard, D. Sugny, B. Lavorel, and O. Faucher, Field-free molecular alignment of CO_2 mixtures in presence of collisional relaxation, *J. Raman Spectrosc.* **39**, 694 (2008).
- [11] N. Owschimikow, F. Königsmann, J. Maurer, P. Giese, A. Ott, B. Schmidt, and N. Schwentner, Cross sections for rotational decoherence of perturbed nitrogen measured via decay of laser-induced alignment, *J. Chem. Phys.* **133**, 044311 (2010).
- [12] D. Pentlehner, J. H. Nielsen, A. Slenczka, K. Mølmer, and H. Stapelfeldt, Impulsive laser induced alignment of molecules dissolved in helium nanodroplets, *Phys. Rev. Lett.* **110**, 093002 (2013).
- [13] L. Christiansen, J. H. Nielsen, D. Pentlehner, J. G. Underwood, and H. Stapelfeldt, Alignment enhancement of molecules embedded in helium nanodroplets by multiple laser pulses, *Phys. Rev. A* **92**, 053415 (2015).
- [14] B. Shepperson, A. A. Søndergaard, L. Christiansen, J. Kaczmarczyk, R. E. Zillich, M. Leshko, and H. Stapelfeldt, Laser-induced rotation of iodine molecules in helium nanodroplets: revivals and breaking free, *Phys. Rev. Lett.* **118**, 203203 (2017).
- [15] A. S. Chatterley, L. Christiansen, C. A. Schouder, A. V. Jørgensen, B. Shepperson, I. N. Cherepanov, G. Bighin, R. E. Zillich, M. Leshko, and H. Stapelfeldt, Rotational coherence spectroscopy of molecules in helium nanodroplets: reconciling the time and the frequency domains, *Phys. Rev. Lett.* **125**, 013001 (2020).

- [16] I. N. Cherepanov, G. Bighin, C. A. Schouder, A. S. Chatterley, S. H. Albrechtsen, A. V. Muñoz, L. Christiansen, H. Stapelfeldt, and M. Leshko, Excited rotational states of molecules in a superfluid, *Phys. Rev. A* **104**, L061303 (2021).
- [17] J. P. Toennies and A. F. Vilesov, Superfluid helium droplets: a uniquely cold nanomatrix for molecules and molecular complexes, *Angew. Chem. Int. Ed.* **43**, 2622 (2004).
- [18] M. Y. Choi, G. E. Douberly, T. M. Falconer, W. K. Lewis, C. M. Lindsay, J. M. Merritt, P. L. Stiles, and R. E. Miller, Infrared spectroscopy of helium nanodroplets: novel methods for physics and chemistry, *Int. Rev. Phys. Chem.* **25**, 15 (2006).
- [19] Y. Kwon, P. Huang, M. V. Patel, D. Blume, and K. B. Whaley, Quantum solvation and molecular rotations in superfluid helium clusters, *J. Chem. Phys.* **113**, 6469 (2000).
- [20] See Supplemental Material for details on experimental methods, analysis and the calculations, which includes Refs. [46-49].
- [21] R. Dörner, V. Mergel, O. Jagutzki, L. Spielberger, J. Ullrich, R. Moshammer, and H. Schmidt-Böcking, Cold target recoil ion momentum spectroscopy: a ‘momentum microscope’ to view atomic collision dynamics, *Phys. Rep.* **330**, 95 (2000).
- [22] J. Ullrich, R. Moshammer, R. Dorn, R. Dörner, L. Ph. H. Schmidt, and H. Schmidt-Böcking, Recoil-ion and electron momentum spectroscopy: reaction-microscopes, *Rep. Prog. Phys.* **66**, 1463 (2003).
- [23] B. Shepperson, A. S. Chatterley, A. A. Søndergaard, L. Christiansen, M. Leshko, and H. Stapelfeldt, Strongly aligned molecules inside helium droplets in the near-adiabatic regime, *J. Chem. Phys.* **147**, 013946 (2017).
- [24] A. S. Chatterley, C. Schouder, L. Christiansen, B. Shepperson, M. H. Rasmussen, and H. Stapelfeldt, Long-lasting field-free alignment of large molecules inside helium nanodroplets, *Nat. Commun.* **10**, 133 (2019).
- [25] A. Staudte, S. Patchkovskii, D. Pavičić, H. Akagi, O. Smirnova, D. Zeidler, M. Meckel, D. M. Villeneuve, R. Dörner, M. Y. Ivanov, and P. B. Corkum, Angular tunneling ionization probability of fixed-in-space H_2 molecules in intense laser pulses, *Phys. Rev. Lett.* **102**, 033004 (2009).
- [26] S. F. Zhao, C. Jin, A. -T. Le, T. F. Jiang, and C. D. Lin, Determination of structure parameters in strong-field tunneling ionization theory of molecules, *Phys. Rev. A* **81**, 033423 (2010).
- [27] P. H. Bucksbaum, A. Zavriyev, H. G. Muller, and D. W. Schumacher, Softening of the H_2^+ molecular bond in intense laser fields, *Phys. Rev. Lett.* **64**, 1883 (1990).
- [28] T. Zuo and A. D. Bandrauk, Charge-resonance-enhanced ionization of diatomic molecular ions by intense lasers, *Phys. Rev. A* **52**, R2511 (1995).
- [29] Y. Mi, P. Peng, N. Camus, X. Sun, P. Fross, D. Martinez, Z. Dube, P. B. Corkum, D. M. Villeneuve, A. Staudte, R. Moshammer, and T. Pfeifer, Clocking enhanced ionization of hydrogen molecules with rotational wave packets, *Phys. Rev. Lett.* **125**, 173201 (2020).
- [30] J. Mikosch, C. Z. Bisgaard, A. E. Boguslavskiy, I. Wilkinson, and A. Stolow, The quantitative determination of laser-induced molecular axis alignment, *J. Chem. Phys.* **139**, 024304 (2013).

- [31] M. Fárník and J. P. Toennies, Ion-molecule reactions in ^4He droplets: Flying nano-cryo-reactors, *J. Chem. Phys.* **122**, 014307 (2004).
- [32] A. Przystawik, A. Kickermann, A. Al-Shemmary, S. Düsterer, A. M. Ellis, K. von Haeften, M. Harmand, S. Ramakrishna, H. Redlin, L. Schroedter, M. Schulz, T. Seideman, N. Stojanovic, J. Szekely, F. Tavella, S. Toleikis, and T. Laarmann, Generation of the simplest rotational wave packet in a diatomic molecule: Tracing a two-level superposition in the time domain, *Phys. Rev. A* **85**, 052503 (2012).
- [33] J. Komasa, K. Piszczatowski, G. Łach, M. Przybytek, B. Jeziorski, and K. Pachucki, Quantum electrodynamics effects in rovibrational spectra of molecular hydrogen, *J. Chem. Theory Comput.* **7**, 3105 (2011).
- [34] A. de Lange, G. D. Dickenson, E. J. Salumbides, W. Ubachs, N. de Oliveira, D. Joyeux, and L. Nahon, VUV Fourier-transform absorption study of the Lyman and Werner bands in D_2 , *J. Chem. Phys.* **136**, 234310 (2012).
- [35] D. E. Jennings, A. Weber, and J. W. Brault, Raman spectroscopy of gases with a Fourier transform spectrometer: the spectrum of D_2 , *Appl. Opt.* **25**, 284(1986).
- [36] M. Hartmann, R. E. Miller, J. P. Toennies, and A. Vilesov, Rotationally resolved spectroscopy of SF_6 in liquid helium clusters: A molecular probe of cluster temperature, *Phys. Rev. Lett.* **75**, 1566 (1995).
- [37] S. Grebenev, M. Hartmann, M. Havenith, B. Sartakov, J. P. Toennies, and A. F. Vilesov, The rotational spectrum of single OCS molecules in liquid ^4He droplets, *J. Chem. Phys.* **112**, 4485 (2000).
- [38] I. F. Silvera, The solid molecular hydrogens in the condensed phase: Fundamentals and static properties, *Rev. Mod. Phys.* **52**, 393 (1980).
- [39] Y. Y. Milenko, R. M. Sibileva, and M. A. Strzhemechny, Natural ortho-para conversion rate in liquid and gaseous hydrogen, *J. Low Temp. Phys.* **107**, 77 (1997).
- [40] K. Urano and K. Motizuki, Ortho-para conversion of H_2 and D_2 diluted in solid HD, *Solid State Commun.* **5**, 691 (1967).
- [41] M. Blancafort-Jorquera, A. Vilà, and M. González, Rotational energy relaxation quantum dynamics of a diatomic molecule in a superfluid helium nanodroplet and study of the hydrogen isotopes case, *Phys. Chem. Chem. Phys.* **21**, 21007 (2019).
- [42] M. Hartmann, F. Mielke, J. P. Toennies, A. F. Vilesov, and G. Benedek, Direct spectroscopic observation of elementary excitations in superfluid He droplets, *Phys. Rev. Lett.* **76**, 4560 (1996).
- [43] K. Nauta and R. E. Miller, The vibrational and rotational dynamics of acetylene solvated in superfluid helium nanodroplets, *J. Chem. Phys.* **115**, 8384 (2001).
- [44] Perhaps with the exception of the HF molecule (Ref. [45]).
- [45] K. Nauta and R. E. Miller, Metastable vibrationally excited HF ($v=1$) in helium nanodroplets, *J. Chem. Phys.* **113**, 9466 (2000).
- [46] A. Braun and M. Drabbels, Photodissociation of alkyl iodides in helium nanodroplets. I. Kinetic energy transfer, *J. Chem. Phys.* **127**, 114303 (2007).
- [47] A. Khan, T. Jahnke, S. Zeller, F. Trinter, M. Schöffler, L. Ph. H. Schmidt, R. Dörner, and M. Kunitski, Visualizing the geometry of hydrogen dimers, *J. Phys. Chem. Lett.* **11**, 2457 (2020).
- [48] F. M. Tao, An accurate ab initio potential energy surface of the He- H_2 interaction,

J. Chem. Phys. **100**, 4947 (1994).

[49] M. Leshko, Quasiparticle approach to molecules interacting with quantum solvents, Phys. Rev. Lett. **118**, 095301 (2017).

Supplemental Material:

Femtosecond rotational dynamics of D₂ molecules in superfluid helium nanodroplets

Junjie Qiang,¹ Lianrong Zhou,¹ Peifen Lu,¹ Kang Lin,¹ Yongzhe Ma,¹ Shengzhe Pan,¹
Chenxu Lu,¹ Wenyu Jiang,¹ Fenghao Sun,¹ Wenbin Zhang,¹ Hui Li,¹ Xiaochun
Gong,¹ Ilya Sh. Averbukh,² Yehiam Prior,^{1,2} Constant A. Schouder,³ Henrik
Stapelfeldt,³ Igor N. Cherepanov,⁴ Mikhail Lemesko,⁴ Wolfgang Jäger,⁵ Jian Wu^{1,6,7}

¹*State Key Laboratory of Precision Spectroscopy, East China Normal University, Shanghai 200241, China*

²*AMOS and Department of Chemical Physics, Weizmann Institute of Science, Rehovot 76100, Israel*

³*Department of Chemistry, Aarhus University, Langelandsgade 140, 8000 Aarhus C, Denmark*

⁴*Institute of Science and Technology Austria, Am Campus 1, 3400 Klosterneuburg, Austria*

⁵*Department of Chemistry, University of Alberta, Edmonton, Alberta T6G 2G2, Canada*

⁶*Collaborative Innovation Center of Extreme Optics, Shanxi University, Shanxi 030006, China*

⁷*CAS Center for Excellence in Ultra-intense Laser Science, Shanghai 201800, China*

1. Comparison of the kinetic energy spectra and angular distribution of D⁺ from isolated D₂ and HeD⁺ from in-droplet D₂ molecules.

To illustrate the difference between the fragment ions from ionization of the isolated and the in-helium D₂ molecules, we compare the kinetic energy (E_{kin}) spectra and angular distributions of the D⁺ and HeD⁺ ions. Figure S1(a) depicts the results for the D⁺ ions, which originate mainly from dissociative ionization of the isolated D₂ molecules. The figure shows that at the intensity of the probe pulse, the D₂(1,0) channel, centered at ~1.7 eV, dominates the spectrum. The strong anisotropy in both the angular distributions of both the D₂(1,0) and the D₂(1,1) channels [inset in Fig. S1(a)] is a result of the molecular alignment-dependent dissociative ionization rate. Figure S1(b) depicts the kinetic energy spectrum of the HeD⁺ ions. We note that the kinetic energies of the HeD⁺ ions are below 1 eV. This shift of the E_{kin} distribution of the HeD⁺ to values much lower than those of the D⁺ ions in the gas-phase spectrum

[shown in Fig. S1(a)] is explained by the energy loss of the D^+ ions (and of HeD^+ ions once they are formed) as they collide with He atoms on their way out of the droplet. The relative loss of E_{kin} is more pronounced than had been observed for heavier iodine fragment ions [1] and is ascribed to a more efficient transfer of kinetic energy in the collisions due to the mass similarity of D^+ and He. The anisotropy of the HeD^+ angular distribution [see inset in Fig. S1(b)] is less pronounced than that of the D^+ ions in the gas phase. Here, too, the observation is ascribed to the fact that collisions between the departing D^+ ions and He atoms will significantly change the initial propagation direction of the D^+ ions. The reduced anisotropy illustrates why the angular distribution of the HeD^+ fragment ions is not a useful observable for characterizing the alignment of D_2 molecules in He droplets.

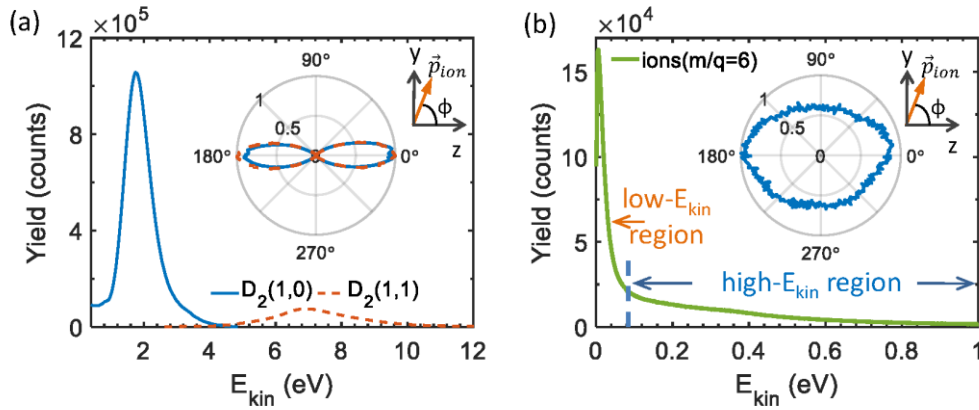


FIG. S1. (a)-(b) Measured E_{kin} spectra and angular distributions (insets) of the photofragment D^+ from the isolated D_2 molecules via the $D_2(1,0)$ (solid blue lines) and $D_2(1,1)$ (orange dashed lines) channels and of the ionic fragment HeD^+ from the in-droplet D_2 molecules. Here, ϕ is the angle of the ejection direction of a fragment ion with respect to the polarization direction of the probe pulse (z -axis). The angular distribution in (b) is extracted for the ionic fragment in the high- E_{kin} region.

2. Origin of the low- E_{kin} fragments with $m/q=6$

Here, we discuss the low- E_{kin} fragments with $m/q=6$ assigned to D_3^+ , as depicted in Fig. S1(b). In our experiments, there was a non-negligible probability that a helium

droplet captured two or more D_2 molecules when passing through the doping cell. Thus, the fragments with $m/q=6$ may also originate from D_3^+ , which is produced via an exoergic reaction $D_2^+ + D_2 \rightarrow D_3^+ + D$ [2] or via a dissociative ionization of D_2 dimers [3], leaving the droplet as a bare ion. The measured low- E_{kin} fragments in Fig. 2(a) and Fig. S1(b) can be assigned to D_3^+ because the momentum of the nascent D_3^+ is much smaller compared to the photofragments D^+ . This is confirmed by the reduced low- E_{kin} /high- E_{kin} yield ratio when the pressure of D_2 molecules in the pick-up cell is decreased. Although the reactions of D_3^+ are supposed to be independent of the molecular alignment, here, the periodical modulation of the time-dependent D_3^+ yield is due to the depletion of D_2^+ by the alignment-sensitive photofragmentation reactions.

3. Determination of the uncertainty of B and D constants from the fit of the experimental data

The frequency resolution of the power spectra (Δf) is mainly determined by the length of the scan time window (T), i.e., $\Delta f = T^{-1} = 1/6 \text{ ps} = 0.167 \text{ THz}$. This frequency resolution, i.e., the smallest frequency division, gives rise to a random error in reading of the central frequencies of the peaks in the power spectra. This random error can usually be one-tenth to one-half of the smallest division. Thus, the random error in reading the central frequencies can range from $\pm 0.02 \text{ THz}$ to $\pm 0.08 \text{ THz}$. Accordingly, we read the central frequencies of the peaks in Fig. 3(c) to the same number of decimal places of the random error, i.e., four peaks of 5.37, 8.94, 12.45 and 15.89 THz for the isolated D_2 molecule and three peaks of 5.35, 8.92 and 12.40 THz for the in-droplet D_2 molecule. Finally, the B and D constants with 95% confidence bounds are obtained by fitting these data points [blue circle, in Figs. 3(d)-(e)], to $B(4J + 6) - D(8J^3 + 36J^2 + 60J + 36)$ using the least square method. For the isolated D_2 molecule, the best fit is obtained for $B_{gas} = 29.98 \pm 0.13 \text{ cm}^{-1}$ and $D_{gas} = 0.013 \pm 0.004 \text{ cm}^{-1}$, and for the in-droplet D_2 molecule, the best fit is obtained for $B_{He} = 29.9 \pm 1.3 \text{ cm}^{-1}$ and $D_{He} = 0.013 \pm 0.060 \text{ cm}^{-1}$.

4. Simulated and experimental results for isolated D₂ molecules

We calculated the degree of alignment $\langle \cos^2 \theta \rangle(t)$ by solving the time-dependent rotational Schrödinger equation using the B_{gas} and D_{gas} values from the fit of the experimental data. Here, θ is the angle between the alignment pulse polarization direction and the D₂ internuclear axis. The calculation was averaged over the initially populated rotational states, given by a Boltzmann distribution at T=295 K. In our experiments, the probe pulse (z-polarized) is perpendicularly polarized to the pump pulse (y-polarized). As a result, the time-dependent D⁺ yield for isolated D₂ molecules is expected to be proportional to the degree of alignment along the z-direction. For a better comparison between the calculated and the experimental results, we plot $\frac{1}{2}(1 - \langle \cos^2 \theta \rangle(t))$ (dotted blue curve) in Fig. S2(a), which has a strong resemblance with the measured time-dependent yield of D⁺ from the D₂(1,0) channel of isolated gas-phase D₂ molecules (solid red curve). Figure S2(b) depicts the corresponding power spectra of the time-dependent traces in Fig. S2(a). The good agreement between the experimental and calculated results validates the probe method used in our experiment.

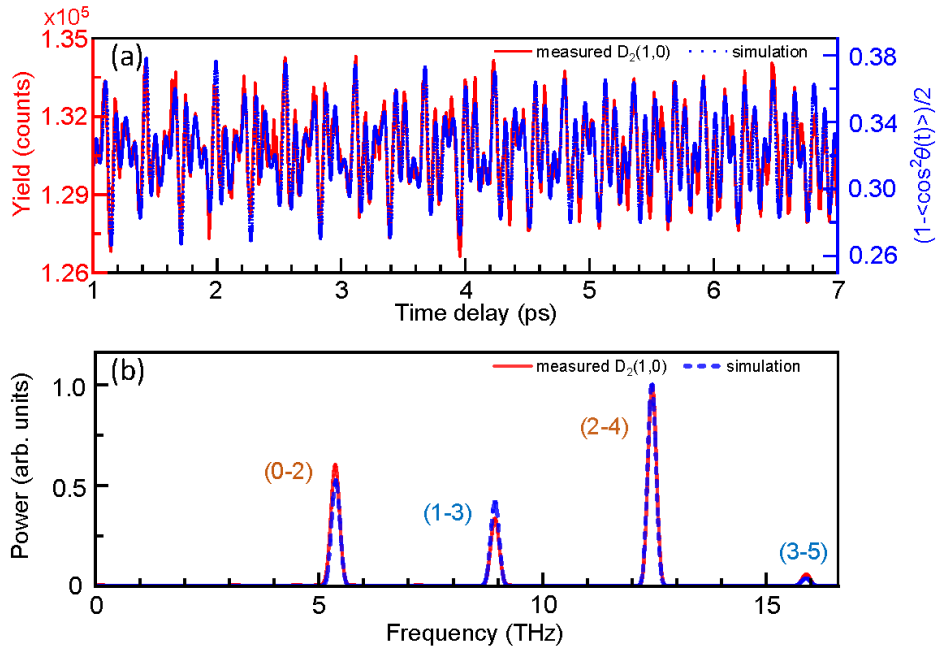


FIG. S2. (a) Calculated degree of alignment along the polarization direction of the probe pulse for D₂ molecules at T=295 K and measured time-dependent yield

trace of D^+ from $D_2(1,0)$ of isolated D_2 molecules. (b) Power spectra corresponding to the two traces in (a).

5. Derivation of the estimate for D_{He}

We use the refined expressions for effective spectroscopic constants obtained within the simplified angulon model in the limit of light rotors [4]

$$\frac{B_{\text{He}}}{B} = 1 - \frac{2u^2}{\Delta_0^2}; D_{\text{He}} = \frac{4B^2u^2}{\Delta_0^3}$$

, where u characterizes the anisotropy of the molecule-helium interaction, $\Delta_0 = \omega + B\lambda(\lambda + 1)$ with $\omega = 6 \text{ cm}^{-1}$ and $\lambda = 2$ being the roton energy and the dominating anisotropic component of the D_2 -He potential energy surface (PES), respectively. Inspecting the H_2 -He PES [5], we estimated $u = 1.3 \text{ cm}^{-1}$ as defined in Ref. [6]. Substituting the parameters into the equation, we obtain $D_{\text{He}} = 0.001 \text{ cm}^{-1}$ and negligible change in B of 0.003 cm^{-1} .

References

- [1] A. Braun and M. Drabbels, Photodissociation of alkyl iodides in helium nanodroplets. I. Kinetic energy transfer, *J. Chem. Phys.* **127**, 114303 (2007).
- [2] M. Fárník and J. P. Toennies, Ion-molecule reactions in ^4He droplets: Flying nano-cryo-reactors, *J. Chem. Phys.* **122**, 014307 (2004).
- [3] A. Khan, T. Jahnke, S. Zeller, F. Trinter, M. Schöffler, L. Ph. H. Schmidt, R. Dörner, and M. Kunitski, Visualizing the geometry of hydrogen dimers, *J. Phys. Chem. Lett.* **11**, 2457 (2020).
- [4] I. N. Cherepanov, G. Bighin, C. A. Schouder, A. S. Chatterley, S. H. Albrechtsen, A. V. Muñoz, L. Christiansen, H. Stapelfeldt, and M. Leshko, Excited rotational states of molecules in a superfluid, *Phys. Rev. A* **104**, L061303 (2021).
- [5] F. M. Tao, An accurate ab initio potential energy surface of the He- H_2 interaction, *J. Chem. Phys.* **100**, 4947 (1994).
- [6] M. Leshko, Quasiparticle approach to molecules interacting with quantum solvents, *Phys. Rev. Lett.* **118**, 095301 (2017).